Extracting Quantitative Insights from Electrochemical Impedance Spectra Using Statistical Methods

Pavle Boškoski[1], Benjamin Königshofer[3], Gjorgji Nusev[1], Aljaž Ostrež[2], and Vanja Subotić[3]

[1] *Jožef Stefan Institute, Jamova cesta 39, Ljubljana, Slovenia*
pavle.boskoski@ijs.si
gjorgji.nusev@gmail.com

[2] *Faculty of Information Studies in Novo mesto, Ljubljanska cesta 31a, Novo mesto, Slovenia*
aljaz.ostrez@student.fis.unm.si

[3] *Institute of Thermal Engineering, Graz University of Technology, Infeldgasse 25b/5, 8010 Graz, Austria*
ben.konigshofer@gmail.com
vanja.subotic@tug.at

ABSTRACT

Statistical analysis of electrochemical impedance spectroscopy data provides a systematic way of detecting changes in electrochemical energy systems. Applying concepts of divergence measures directly on electrochemical impedance spectroscopy data, one can reliably detect and quantify statistically significant changes. The result is a set of highlighted frequency bands where the measured impedance characteristics differ statistically significantly from a reference curve. The approach is evaluated on a solid-oxide electrolyser cell operated under different conditions and proves to be sensitive to even the smallest changes. The complete numerical implementation and corresponding experimental data are available as supplementary material at `https://portal.ijs.si/nextcloud/s/xTa2cmtfxXn2jSz`.

1. INTRODUCTION

In characterizing and online monitoring of electrochemical energy systems, electrochemical impedance spectroscopy (EIS) is the primary source of information (Yang et al., 2020). However, direct analysis of impedance curves for detecting small changes is often challenging. Consequently, various post-processing techniques have been developed, for instance, distribution of relaxation times (DRT) and equivalent circuit model (ECM). As a result, the changes of the EIS curves are quantified through changes in the model parameters. Despite the effectiveness of these approaches, a logical question arises: Can the analysis of impedance data be performed in a more direct approach without introducing additional models?

There are two main challenges with the current approaches for analyzing EIS curves. The first is the limited number of measured data points. EIS is typically performed using (multi-)sine excitation that results in no more than a dozen points per decade. With such a low cardinality data set, any task of model fitting almost always becomes ill-posed, i.e., the number of the model parameters is comparable to the size of the data set. This is usually resolved by introducing regularisation parameters (Papurello, Menichini, & Lanzini, 2017; Wan, Saccoccio, Chen, & Ciucci, 2015; Effat & Ciucci, 2017).

The second challenge is that electrochemical energy systems belong to a particular group of linear systems called fractional-order systems (Sadli et al., 2010). These linear systems include a concept of non-integer derivation order, hence the name. The biggest challenge when performing identification of such systems is the still-open issue of structural identification, i.e., determining the most suitable model based on the available information in the acquired signals. In the context of integer-order linear systems, structural identification determines the number of poles of the system or, in terms of ECM, the number of RC elements (Overschee & Moor, 1993). For fractional-order systems, in addition to the number of poles, one also needs the power of the pole, i.e., the

fractional order $\alpha \in \mathbb{R}^+$ (Lasia, 2014; Monje, Chen, Vinagre, Xue, & Feliu-Batlle, 2010). In a lack of a proper approach, there is the pressing issue of determining the most suitable structure of an ECM for the system at hand (Ciucci, 2019). This is the main reason why DRT analysis has gained a lot of traction in the field of fuel cells (Liu & Ciucci, 2020; Effat & Ciucci, 2017; Kobayashi & Suzuki, 2018; Fadaei & Mohammadi, 2015; Subotić et al., 2020).

What is proposed here is a non-parametric approach to analyzing EIS data. The key idea is to track the changes in the statistical properties of impedance at each frequency to a reference one. The concept of statistical analysis of impedance data is a recent one (Boškoski, Debenjak, & Boshkoska, 2017; Stepančič, Juričić, & Boškoski, 2019). However, what is proposed here goes one step further. By using the concept of statistical divergence, it becomes possible not only to detect the frequency bands where the impedance change is statistically significant but also to quantify that change.

The proposed approach involves three steps: impedance calculation through continuous wavelet transform (CWT) (Boškoski et al., 2017), estimation of the probability density of impedance at a desired set of frequencies, and applying divergence measures to a reference measurement to quantify the change of the impedance values. This is an entirely new way of analyzing impedance data. Therefore, each step in the data analysis is described in a separate section for proper presentation. Section 2 presents the basic concepts of statistical divergence. Section 3 describes the signal processing step required to obtain impedance data in such a form so that the divergence concept becomes applicable. Finally, Sections 4 and 5 contain the experimental setup and complete results obtained by characterizing solid-oxide electrolyser cell (SOEC) under various operating conditions. The complete numerical implementation is available as supplementary material and is described in Appendix 6.

2. STATISTICAL ANALYSIS

The main goal of analyzing EIS data is to determine the frequencies where the impedance characteristic exhibits significant changes and to quantify those changes. In the context of fuel cells, external influences, such as gas flows, fuel compositions, and environmental parameters, affect the system's dynamics. Furthermore, the inherent diffusion phenomena are stochastic on the microscale despite having close to deterministic properties on the macroscale. As a result, it becomes possible to exploit the stochastic nature of electrochemical energy systems to quantify any significant changes in their behavior.

Tools for detecting significant changes in the statistics of stochastic signals are readily available. Most prominent concepts include hypothesis testing such as Kolmogorov-Smirnov test, Adam test, and many more (Wasserman, 2006). The concept of divergence goes one step further and provides a way of quantifying those changes. The most commonly used divergences are Kullback-Leibler (KL) divergence and Rényi divergence (Pardo, 2005). The divergence-based approaches solve the problem of detecting and quantifying statistically significant changes in EIS curves.

2.1. Definition of divergence

There are two ways of calculating divergence. The first method is based on constructing probability density estimations from statistical samples. The second method is based on constructing histograms.

Definition 2.1. *Let S be the space of all probability distributions with common support (i.e., all distributions in S have non-zero values on the common support).* ***Divergence*** *is the function $D(\cdot\|\cdot) : S \times S \to \mathbb{R}$, such that:*

1. $D(p\|q) \geq 0$ *for all* $p, q \in S$,
2. $D(p\|q) = 0 \Leftrightarrow p = q$.

Dual divergence D^* *is defined as* $D^*(p\|q) = D(q\|p)$.

Divergence is not necessarily symmetric and unaffected by triangle inequality, so it cannot be equated with a metric. Several different divergences have been defined. Most of them have beneficial properties for our data analysis (e.g., one divergence is more sensitive to the mean value of the distributions, and the other divergence is more sensitive to the variance of the distributions).

There are several variations of divergence definitions:

1. **Rény divergence divergence**:

$$D_\alpha(P\|Q) = \frac{1}{\alpha - 1} \cdot \log \int_\Omega \Big(p(x)\Big)^\alpha \Big(q(x)\Big)^{1-\alpha} \, dx. \tag{1}$$

   where p and q are probability density functions with support Ω and $\alpha > 0$.

2. **f-divergence**: This is a family of divergences generated by the function f, such that:
   - f is convex on $\mathbb{R}^+$,
   - $f(1) = 0$.

   The elements of this family are:

$$D_f(p\|q) = \int_\Omega p(x) \cdot f\Big(\frac{p(x)}{q(x)}\Big) \, dx, \tag{2}$$

   where p and q are probability density functions with support Ω.

3. **Hellinger distance**:

$$H^2(p, q) = 2 \int_\Omega \Big(\sqrt{p(x)} - \sqrt{q(x)}\Big)^2 \, dx, \tag{3}$$

   where p and q are probability density functions with support Ω.

The above formulas are valid for continuous variables. The formula for discrete variables is analogous.

Rényi divergence is a more general form of the KL divergence. The complete derivation is defined for continuous variables since the definition of discrete is analogous. Rényi divergence is not defined in $\alpha = 1$, but we know its limit in this point:

Theorem 2.1. *Let $D_\alpha(P\|Q)$ be Rényi divergence of distributions P and Q. Then the following applies:*

$$\lim_{\alpha\to 1} D_\alpha(P\|Q) = \int_\Omega p(x)\cdot\log\left(\frac{p(x)}{q(x)}\right)dx, \qquad (4)$$

*where the expression on the right is exactly **Kullback-Leibler divergence** of distributions P and Q, i.e.*

$$\lim_{\alpha\to 1} D_\alpha(P\|Q) = D_{KL}(P\|Q). \qquad (5)$$

3. EIS WITH STOCHASTIC EXCITATION

To apply divergence measures described in Section 2, one has to be able to estimate the probability distribution of the impedance at selected frequencies. Standard EIS approaches that typically rely on the Fourier transform provide only time average estimates of the impedance values within the observation window. Furthermore, such EIS is evaluated on a discrete frequency set, typically having a dozen points per decade.

Using fast EIS with stochastic excitation provides an almost continuous frequency interval (Boškoski et al., 2017). Furthermore, having time-frequency evolution of the impedance characteristics, it is possible to estimate the probability distributions of the measured impedance at the observed frequencies (Nusev, Juričić, Gaberšček, Moškon, & Boškoski, 2021; Boškoski & Debenjak, 2014). It is shown that the distribution of the complex impedance at a particular frequency is:

$$f_Z(z) = \frac{1-|\rho|^2}{\pi\sigma_u^2\sigma_i^2}\left(\frac{|z|^2}{\sigma_u^2}+\frac{1}{\sigma_i^2}-2\frac{\rho_r z_r-\rho_i z_i}{\sigma_u\sigma_i}\right)^{-2}, \qquad (6)$$

where z_r and z_i are real and imaginary components of the random variable Z. The location of the $f_Z(z)$ mode depends on the correlation coefficient ρ. From (6), one can also derive the distributions of the real and imaginary parts.

Any electrochemical system can be safely considered deterministic on a macroscopic scale despite having stochastic governing mechanisms on a microscopic scale. Therefore, in the fast EIS approach, the primary source of stochastic properties stems from the stochastic excitation and the observation noise. If the excitation signal is the current, this means that the parameter σ_i is known a-priori. However, any changes in the observed system directly affect the observed output voltage, i.e., σ_u, and the complex correlation at a particular frequency ρ. Under such changes, the actual shape of the distribution (6) will change. Therefore, one can detect any changes in the observed system by simply tracking σ_u and ρ.

This can be achieved quite efficiently through divergence measures. Assuming that the system can be safely considered nominal at a starting point in time, one can quantify changes in the statistical properties of impedance at a particular frequency relative to this reference measurement. Although the values of the parameters σ_u, σ_i and ρ can be easily estimated, calculating the KL divergence (5) for two distributions (6) might be challenging. Consequently, the KL divergence (5) can be empirically estimated from the histograms of the impedance components.

4. EXPERIMENTAL SETUP

Several SOEC in an industrial size (100 cm^2) were employed for experimental investigations of the proposed divergence measures. The cells were tested in a ceramic cell housing to avoid any external influences on the operating cell. Thus, all the results observed can be correlated directly to the cell under investigation and its environment.

Ni-mesh was employed to contact the fuel electrode, and platinum was used as a current collector on the air electrode. The fuel electrode was fed with two different fuel mixtures, containing H_2 and H_2O, in ratios of 20/80 and 10/90, respectively. The set of operating conditions is shown in Table 1. The impact of the varying hydrogen and steam quantities on the electrolysis processes and hydrogen generation was thus examined. Moreover, the impact of their ratio on performance degradation was investigated. Next, the operating current was varied from OCV up to the critical voltage value, defined as 1.35 V. Operating the cell beyond its limit enables a deeper insight into the electrochemical processes and degradation mechanisms. Furthermore, the operating temperature was controlled to be the constant 835°C in the furnace. During the experiment, the temperature inside the cell was measured on altogether 12 points inside the cell (as shown in Figure 1 for one electrode side). In addition, temperature was measured in the inlet and outlet gas pipes and the furnace. The analysis of the gas mixture at both electrodes' inlet and outlet was continuously performed using gas analyzers.

The polarization curve and electrochemical impedance spectroscopy were measured in a galvanostatic mode. The EIS measurements were carried out by superimposing the discrete random binary sequence (DRBS) perturbated AC-current to the DC-current. The amplitude of the AC-current was 4% of the DC.

4.1. Measurement loop

For EIS, a custom-made voltage-controlled current source power supply module was used (Petrovčič, Černe, & Dolanc, 2020). The power supply can provide currents up to 100 A

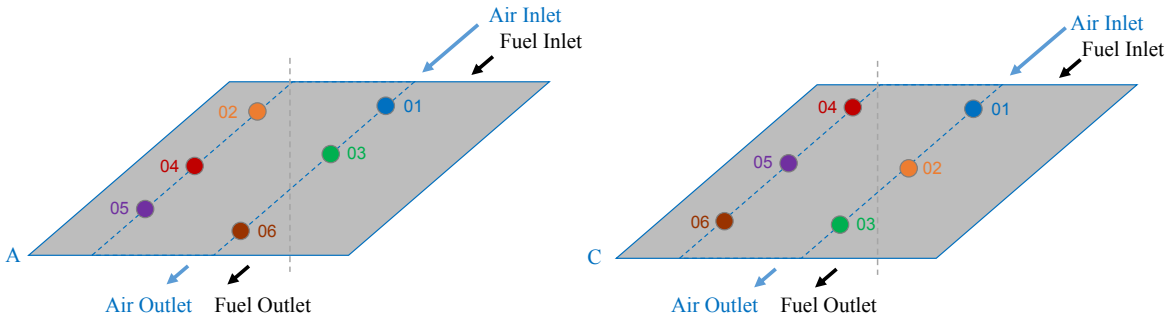

Figure 1. Position of thermocouples for temperature measurement on the anode (A) and cathode (C).

Table 1. Operating parameters

Label	Current Density mA/cm^2	Fuel Flow SLPM	H_2 %	H_2O %	Air Flow SLPM	Temperature °C
Condition 1	700	2.125	20	80	2.267	835
Condition 2	700	1.889	10	90	2.267	835
Condition 3	900	2.125	20	80	2.267	810

for voltages up to 5V in the frequency range between 0 and 20kHz (the upper frequency depends on the load impedance under test). In order to cover the frequency spectrum of interest between 0.1 Hz and 10 kHz 6 different DRBS excitation signals were used with $f_B \in$\{0.1 Hz, 1 Hz, 10 Hz, 100 Hz, 1 kHz, 10 kHz\}. The length of each of the DRBS signals is 200, 120, 45, 6, 2.3, and 1.3 seconds, respectively. Current is measured using CAENels CT-100-V flux-gate current transducer. The voltage response of the cell under test and the measured current were sampled differentially using an NI USB-6216 card, which has a 16-bit ADC. DRBS signals with f_B up to 10 Hz, were sampled with f_s=30 kHz. The perturbation with higher f_B was sampled with f_s=150 kHz.

5. RESULTS

The evaluation of the non-parametric change detection of EIS curves was evaluated on data acquired on SOEC under various operating conditions, as listed Table 1. The operating parameter changes were chosen to obtain a more detailed insight into the performance SOEC. Each operating condition listed in Table 1 is analyzed separately. During each section, all gas flows were kept constant.

For each operating condition, three groups of results are presented. The first group consists of the time evolution of the cell's voltage and 6+6 temperatures measured in two points, A and B, as shown in Figure 1. The plots show the relative temperature change over time to the temperature measured at $t = 0$ for each operating condition separately. The second group includes the time evolution of EIS curves. Since EIS measurements were performed every 4 hours, there are at least 15 curves for each operating condition. The initial and the last EIS curves are marked with red and blue lines, respectively. The final third group is the results from the proposed KL divergence-based approach, providing information on the severity of the changes in the EIS curve.

5.1. Operating condition 1

In this condition, the SOEC was operating for 60 hours. The evolution of the cell voltage and temperatures at anode side (A) and cathode side (C) (see Figure 1) are shown in Figure 2a. The periodic EIS measurements are seen as abrupt scalar value changes. The cell's voltage and the temperatures measured at the cathode show a clear decrease trend. The temperatures on the anode are almost constant.

The impedance evolution is shown in Figure 2b. There are noticeable changes in the low-frequency bands. Also, there are changes in the serial resistance, although it is smaller. On the other one could assume that there are no significant changes in the EIS curves at frequencies above 10 Hz.

The KL divergence results are shown in Figure 2c. It shows a continuous increase of the divergence in the frequency band between 0.3 – 2 Hz after approximately 20 hours of operation, which is in line with the changes in the Nyquist plot. This can be interpreted as diffusion losses according to (Fang, Blum, & Menzler, 2015). A similar high degree of divergence is observable at frequencies between 10 – 40 Hz after approximately 40 hours of operation, whereby the processes at frequencies between 10 – 100 Hz are linked to changes in the air electrode processes like chemical surface exchange of O_2 and $O_2{}^{2-}$-bulk diffusion in air electrode according to (Leonide, Sonn, Weber, & Ivers-Tiffée, 2008) and (Sonn, Leonide, & Ivers-Tiffée, 2008). Generally, the changes presented in these figures could be interpreted as the stabilization of processes linked to an increasing amount of hydrogen during the initial operational period.

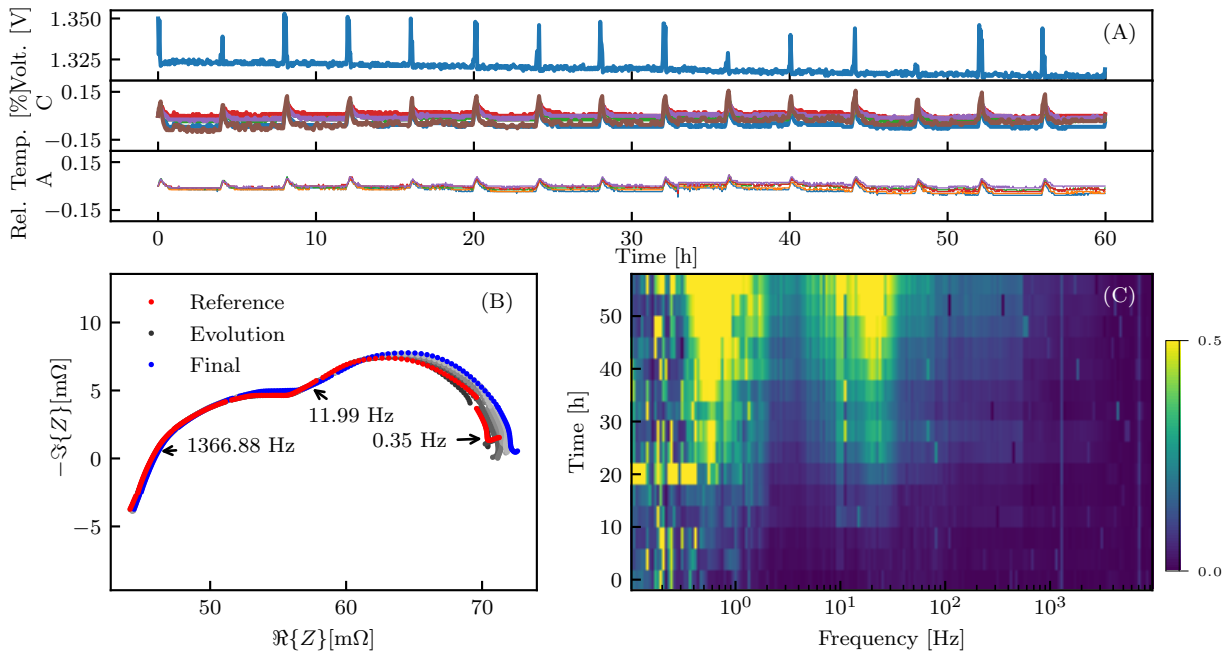

Figure 2. Results of operation under condition 1. Group (A) shows the time evolutions of the voltage and relative change of the temperatures at the anode-A and cathode-C sides. The relative change of the temperatures is calculated based on the initial measurement at $t = 0$. The local abrupt changes in the voltage and temperature values occur during the periodic EIS measurements. Plot (B) shows the evolution of the EIS curves from red to blue. Plot (C) shows the results of KL divergence evolution over the 60 hours during condition 1. The divergences are calculated to the reference (red) EIS curve. The most pronounced changes in the EIS are the frequency bands below 1Hz and between 10 and 100Hz.

5.2. Operation with low hydrogen content: Condition 2

For the case with low hydrogen content, the SOEC operated with 10% hydrogen in the inlet gas mixture. This phase lasted for 85 hours. As shown in Figure 3, there are no significant changes in the temperatures at both measurement points. An apparent initial decrease in the cell's voltage, particularly during the first 40 hours.

The Nyquist plots, shown in the Figure 3b, exhibit a clear trend from the initial measurement (red color) towards the end measurement (blue color). At first glance, the EIS curves exhibit changes throughout the observed frequency band. However, the most clear change in the serial resistance is visible as a slight decay of the cell's voltage.

Figure 3b shows an apparent change of the impedance in the frequency range between 10 Hz - 4 kHz. Initially, after 40 hours of operation, the most intensive changes are in the frequency band between 200 – 800 Hz. After 70 hours of operation, a similar divergence change occurs at frequencies between 800 Hz – 4 kHz. Only slightly higher divergence values are observable in the frequency range between 10 – 200 Hz. These changes can be linked to the shift of the impedance curve towards lower ohmic resistances from 49.5 to 48.5 mΩ and the behavior of the cell voltage, which mainly remained constant during the initial 20 hours but started to decrease from 1.32 to 1.31 V during ongoing operation. Generally, this can be interpreted as a new equilibrium slowly being achieved after the change in the inlet gas composition.

Additionally, Figure 3c shows increased impedance values scattered at frequencies < 1 Hz. These changes are also visible in the Nyquist diagram, whereby the low-frequency arc presents an unstable behavior. According to (Fang et al., 2015; Leonide et al., 2008; Sonn et al., 2008), this could be linked to changes in the diffusion losses, resulting from surplus H_2O which could still be present within the system from the previous experiment.

5.3. Operation under high current densities: Condition 3

The last operating condition includes a test under high current densities of 900 mA/cm^2. Under such a condition, the SOEC exhibits unstable fluctuations. As shown in Figure 4a, the cell voltage fluctuates between 1.45 and 1.46 V. Similar variations can be observed in the cell temperatures at both measurement points.

Unlike the previous two cases when EIS curves exhibit clear time evolution, the EIS curves from these operating conditions fluctuate over time. This is shown in Figure 4b. In high-frequency regions, it seems that there is no change between the initial and the last EIS curves. Furthermore, there

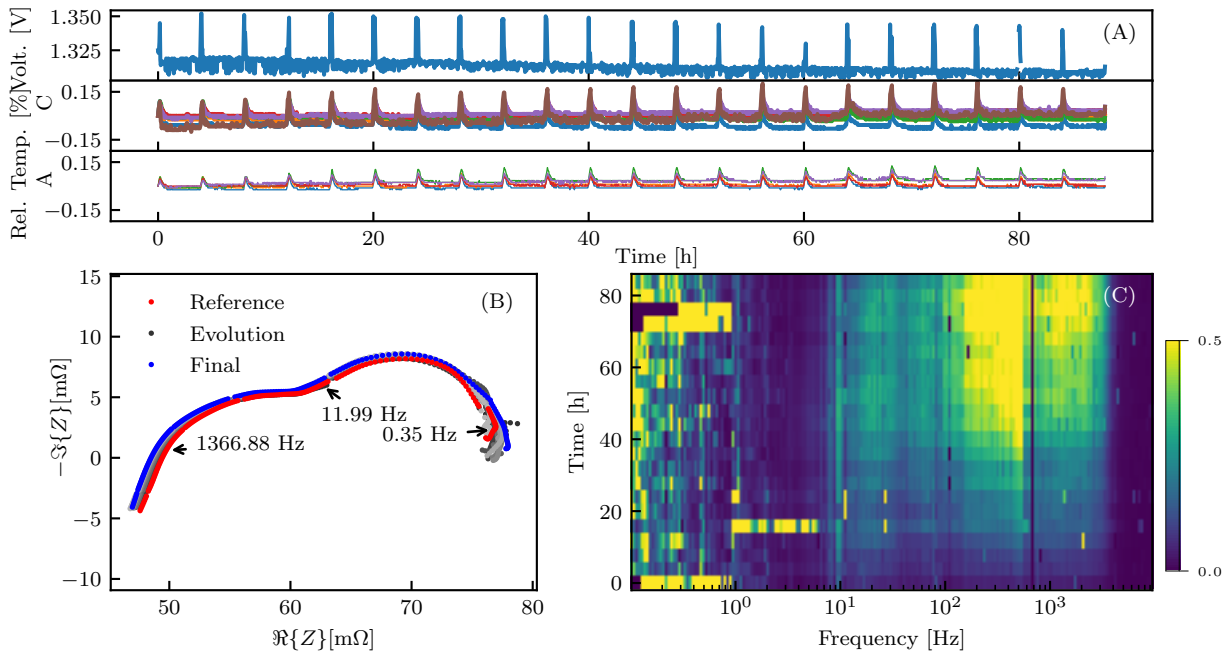

Figure 3. Results of operation under condition 2. Group (A) shows the time evolutions of the voltage and relative change of the temperatures at the anode-A and cathode-C sides. The relative change of the temperatures is calculated based on the initial measurement at $t = 0$. The local abrupt changes in the voltage and temperature values occur during the periodic EIS measurements. Plot (B) shows the evolution of the EIS curves from red to blue. Plot (C) shows the results of KL divergence evolution over the 85 hours during condition 2. The divergences are calculated to the reference (red) EIS curve. The most pronounced EIS changes are in the frequency band between 100 and 2000Hz.

is an apparent variation in the low-frequency region. Under this operating condition, the spectra are noisier than in the previous results. This could also be interpreted as operation instabilities occurring when applying high current densities resulting from the increasing effect of ionic and electronic conduction, activation, and diffusion resistances on the performance (Riedel, Heddrich, & Friedrich, 2019).

When observing the KL results shown in Figure 4c, the fluctuations in the impedance values become more evident. The divergence plot shows pulsating intensity changes at frequencies between 10 and 40 Hz. These changes were identified to be the result of inconsistent steam supply due to pump malfunctioning. This example presents an additional application of this representation since an error source can be detected easily at an early stage, and appropriate countermeasures can be taken to restore the system's normal operation.

5.4. Comparison with distribution of relaxation times and equivalent circuit model

For validation purposes, the results are compared with established tools for analysis of EIS data: DRT and estimation of ECM. Each of the EIS curves from the above cases was analyzed using the DRT tools by (Wan et al., 2015).

When using the Gaussian kernel, the DRT algorithm requires two parameters: the regularisation λ and the shape factor C. For these choices, the optimal values were found as $\lambda = 10^{-5}$ and $C = 3$ (Maradesa, Py, Wan, Effat, & Ciucci, 2023). With these values, the lowest frequency band decade is not visible in the DRT plots. Consequently, the results below 1 Hz can not be directly compared.

The ECM had four RQ elements, i.e., a parallel connection of a resistor and a constant phase element. The transfer function reads as follows:

$$Z(j\omega) = R_s + \sum_{i=1}^{4} \frac{R_i}{1 + (j\omega)^{\alpha} R_i Q_i}. \tag{7}$$

Four poles were selected based on the number of visible peaks in the DRT. After the parameter fitting, it was visible that the most prominent changes were in the values of parameters Q_i. Consequently, only the time evolution of these parameters is shown in the graphs below.

Condition 1 According to results shown in Figure 2, the most prominent changes occur after the 20th hour of operation. These changes are visible in the lowest DRT peak evolution shown in Figure 5a as well as the evolution of the parameter Q_4 shown with green color in Figure 5b.

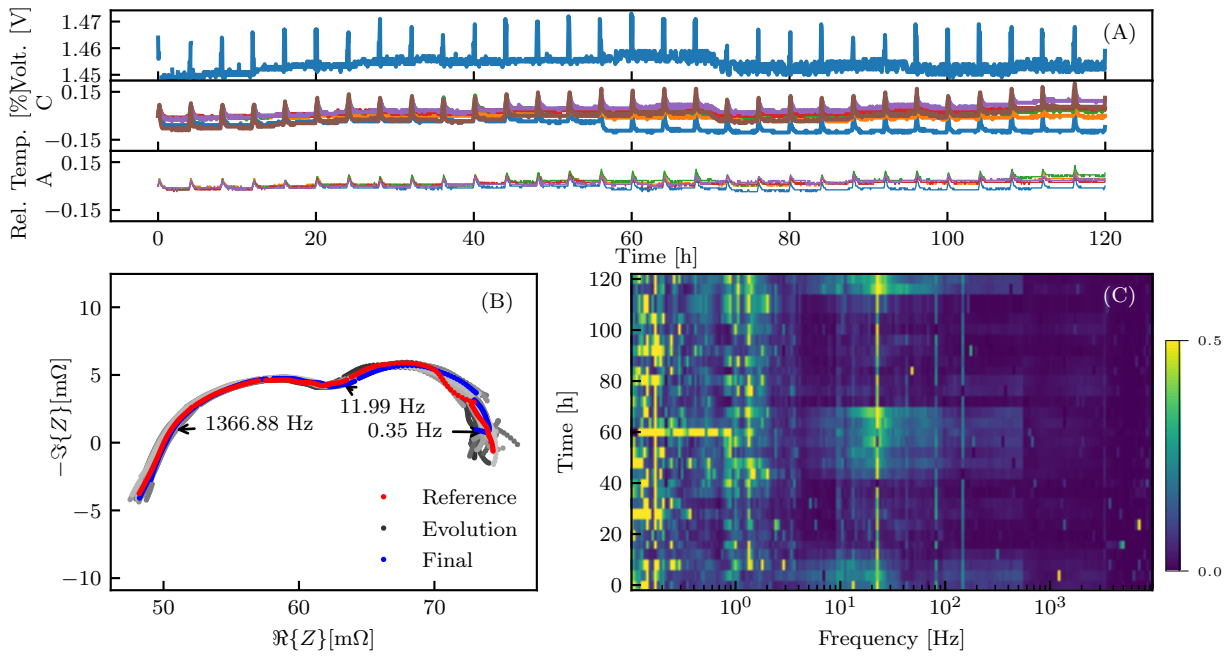

Figure 4. Results of operation under condition 3. Group (A) shows the time evolutions of the voltage and relative change of the temperatures at the anode-A and cathode-C sides. The relative change of the temperatures is calculated based on the initial measurement at $t = 0$. The local abrupt changes in the voltage and temperature values occur during the periodic EIS measurements. Plot (B) shows the evolution of the EIS curves from red to blue. Plot (C) shows the results of KL divergence evolution over the 120 hours during condition 3. The divergences are calculated to the reference (red) EIS curve. Periodic changes in the divergence values around 20Hz are due to malfunctioning steam generation.

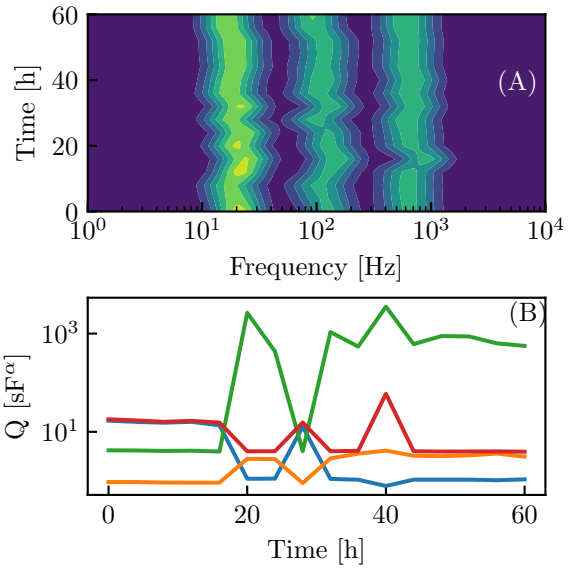

Figure 5. Condition 1

Condition 2 Under low hydrogen content, according to Figure 3, the most prominent changes are visible after the 20th hour of operation in the frequency band above 100 Hz. Similar changes are visible in the second peak of the DRT in Figure 6a as well as three Q_i parameters in Figure 6b.

Condition 3 The case of high current densities is the most complicated. The EIS analysis in Figure 4 shows repetitive changes in the EIS curves occurring in the frequency band above 20 Hz. These intervals are visible in the changes of the first two DRT peaks in Figure 7a. Similar repetitive behavior is visible in two Q_i parameters shown in Figure 7b.

Discussion on the comparison The analysis performed using DRT and ECM leads to the same conclusions as the proposed approach. Two main differences have to be pointed out. Both DRT and ECM undergo an optimization process and selection of hyperparameters. The results of (Maradesa et al., 2023) and (Boškoski, Žnidarič, Gradišar, & Subotić, 2024) provide directions for the optimal selection of required hyperparameters, but their influence is still profound. Furthermore, there is the issue of quantifying the changes in DRT plots and ECM parameters. Conversely, the proposed divergence approach directly provides areas with statistically significant

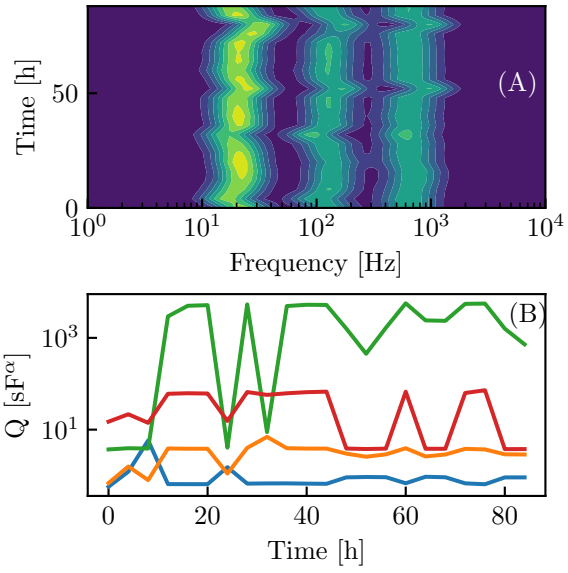

Figure 6. Condition 2

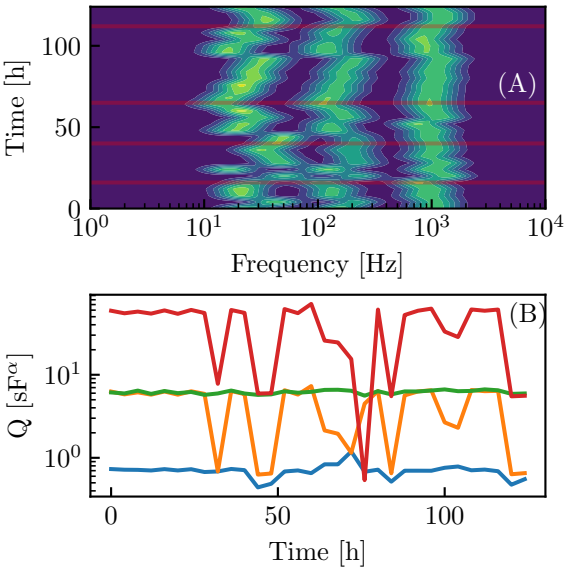

Figure 7. Condition 3

changes, and the calculation does not rely on hyperparameter selection or optimization. As a result, the computational complexity is significantly lower.

6. CONCLUSION

The proposed approach resolves two main issues regarding EIS measurement: detection of frequency intervals where the change occurred and, more importantly, quantifying this change. This is achieved without assuming any impedance models (such as equivalent circuit models), which can be quite challenging for electrochemical systems in general. As a result, the analysis can be performed without any visual inspection of the EIS curves, i.e., it can be fully automated.

This has several practical implications. The numerical implementation of the KL divergence can be done efficiently, thus lowering the computational load. Calculating the fast EIS approach has the same complexity as performing multiple FFTs. Finally, the detection threshold can be easily determined empirically since it depends only on the sample size (duration of the excitation signal). All these properties show the potential of the proposed approach both for laboratory and, more importantly, for online real-world applications.

ACKNOWLEDGEMENTS

The authors acknowledge the Slovenian Research and Innovation Agency's financial support of research core funding No. P2-0001 and research project J2-4452.

REFERENCES

Boškoski, P., Debenjak, A., & Boshkoska, B. M. (2017). *Fast electrochemical impedance spectroscopy*. Springer International Publishing. doi: 10.1007/978-3-319-53390-2

Boškoski, P., & Debenjak, A. (2014, December). Optimal selection of proton exchange membrane fuel cell condition monitoring thresholds. *Journal of Power Sources*, *268*, 692–699. doi: 10.1016/j.jpowsour.2014.06.110

Boškoski, P., Žnidarič, L., Gradišar, v., & Subotić, V. (2024, December). Probabilistic deconvolution for electrochemical impedance through variational bayesian inference. *Journal of Power Sources*, *622*, 235359. Retrieved from http://dx.doi.org/10.1016/j.jpowsour.2024.235359 doi: 10.1016/j.jpowsour.2024.235359

Ciucci, F. (2019, feb). Modeling electrochemical impedance spectroscopy. *Current Opinion in Electrochemistry*, *13*, 132–139. doi: 10.1016/j.coelec.2018.12.003

Effat, M. B., & Ciucci, F. (2017, sep). Bayesian and hierarchical bayesian based regularization for deconvolving the distribution of relaxation times from electrochemical impedance spectroscopy data. *Electrochimica Acta*,

247, 1117–1129. doi: 10.1016/j.electacta.2017.07.050

Fadaei, M., & Mohammadi, R. (2015, dec). A comprehensive simulation of gas concentration impedance for solid oxide fuel cell anodes. *Energy Conversion and Management*, *106*, 93–100. doi: 10.1016/j.enconman.2015.08.073

Fang, Q., Blum, L., & Menzler, N. H. (2015). Performance and degradation of solid oxide electrolysis cells in stack. *Journal of The Electrochemical Society*, *162*, F907-F912. doi: 10.1149/2.0941508jes

Kobayashi, K., & Suzuki, T. S. (2018, sep). Distribution of relaxation time analysis for non-ideal immittance spectrum: Discussion and progress. *Journal of the Physical Society of Japan*, *87*(9), 094002. doi: 10.7566/jpsj.87.094002

Lasia, A. (2014). *Electrochemical impedance spectroscopy and its applications*. Springer New York. doi: 10.1007/978-1-4614-8933-7

Leonide, A., Sonn, V., Weber, A., & Ivers-Tiffée, E. (2008). Evaluation and modeling of the cell resistance in anode-supported solid oxide fuel cells. *Journal of The Electrochemical Society*, *155*, B36. doi: 10.1149/1.2801372

Liu, J., & Ciucci, F. (2020, jan). The gaussian process distribution of relaxation times: A machine learning tool for the analysis and prediction of electrochemical impedance spectroscopy data. *Electrochimica Acta*, *331*, 135316. doi: 10.1016/j.electacta.2019.135316

Maradesa, A., Py, B., Wan, T. H., Effat, M. B., & Ciucci, F. (2023, March). Selecting the regularization parameter in the distribution of relaxation times. *Journal of The Electrochemical Society*, *170*(3), 030502. Retrieved from http://dx.doi.org/10.1149/1945-7111/acbca4 doi: 10.1149/1945-7111/acbca4

Monje, C. A., Chen, Y., Vinagre, B. M., Xue, D., & Feliu-Batlle, V. (2010). Fractional-order systems and controls: fundamentals and applications. In (chap. Chapter 13: Numerical Issues and MATLAB Implementations for Fractional-order Control Systems). Springer Science & Business Media.

Nusev, G., Juričić, Đ., Gaberšček, M., Moškon, J., & Boškoski, P. (2021). Fast impedance measurement of li-ion battery using discrete random binary excitation and wavelet transform. *IEEE Access*, *9*, 46152–46165. doi: 10.1109/access.2021.3058368

Overschee, P. V., & Moor, B. D. (1993). Subspace algorithms for the stochastic identification problem. *Automatica*, *29*(3), 649 - 660.

Papurello, D., Menichini, D., & Lanzini, A. (2017). Distributed relaxation times technique for the determination of fuel cell losses with an equivalent circuit model to identify physicochemical processes. *Electrochimica Acta*, *258*, 98 - 109. doi: 10.1016/j.electacta.2017.10.052

Pardo, L. (2005). *Statistical Inference Based on Divergence Measures*. Abingdon: CRC Press.

Petrovčič, J., Černe, S., & Dolanc, G. (2020). *Power supply unit with diagnostic capabilities* (Tech. Rep.). EU Horizon 2020. doi: 10.3030/735533

Riedel, M., Heddrich, M. P., & Friedrich, K. A. (2019, 2). Analysis of pressurized operation of 10 layer solid oxide electrolysis stacks. *International Journal of Hydrogen Energy*, *44*, 4570-4581. doi: 10.1016/j.ijhydene.2018.12.168

Sadli, I., Urbain, M., Hinaje, M., Martin, J.-P., Raël, S., & Davat, B. (2010, dec). Contributions of fractional differentiation to the modelling of electric double layer capacitance. *Energy Conversion and Management*, *51*(12), 2993–2999. doi: 10.1016/j.enconman.2010.06.045

Sonn, V., Leonide, A., & Ivers-Tiffée, E. (2008). Combined deconvolution and cnls fitting approach applied on the impedance response of technical ni/8ysz cermet electrodes. *Journal of The Electrochemical Society*, *155*, B675. doi: 10.1149/1.2908860

Stepančič, M., Juričić, Đ., & Boškoski, P. (2019, sep). Fault detection of fuel cell systems based on statistical assessment of impedance data. *Energy Conversion and Management*, *195*, 76–85. doi: 10.1016/j.enconman.2019.05.004

Subotić, V., Königshofer, B., Đani Juričić, Kusnezoff, M., Schröttner, H., Hochenauer, C., & Boškoski, P. (2020). Detailed insight into processes of reversible solid oxide cells and stacks using drt analysis. *Energy Conversion and Management*, *226*, 113509. doi: 10.1016/j.enconman.2020.113509

Wan, T. H., Saccoccio, M., Chen, C., & Ciucci, F. (2015). Influence of the discretization methods on the distribution of relaxation times deconvolution: Implementing radial basis functions with drttools. *Electrochimica Acta*, *184*, 483 - 499. doi: 10.1016/j.electacta.2015.09.097

Wasserman, L. (2006). *All of nonparametric statistics*. Springer New York. doi: 10.1007/0-387-30623-4

Yang, B., Wang, J., Zhang, M., Shu, H., Yu, T., Zhang, X., ... Sun, L. (2020). A state-of-the-art survey of solid oxide fuel cell parameter identification: Modelling, methodology, and perspectives. *Energy Conversion and Management*, *213*, 112856. doi: 10.1016/j.enconman.2020.112856

SUPPLEMENTARY MATERIAL: NUMERICAL IMPLEMENTATION

The numerical implementation of the presented method is available at https://portal.ijs.si/nextcloud/s/xTa2cmtfxXn2jSz. The main implementation is presented with Python Jupyter notebook KL_GPU.ipynb. The above repository contains the re-

quired supplementary `Python` scripts. The data sets are stored as `NumPy` files. The complete data set is approximately 2 GB. Pre-processed data are stored as `all_KL_hist.npz`.